A New Form of Nanosized $SrTiO_3$ Material for Near-Human-Body Temperature Oxygen Sensing Applications

Y. Hu,[†] O. K. Tan,*[,†] J. S. Pan,[‡] and X. Yao[§]

Sensors & Actuators Lab, Microelectronics Centre, School of EEE, Nanyang Technological University, 50 Nanyang Avenue, Singapore 639798, Singapore, Institute of Materials Research and Engineering, Singapore 117602, Singapore, and Electronic Materials Research Laboratory, Xian Jiaotong University, Xian 710049, P.R. China

Received: March 8, 2004; In Final Form: May 9, 2004

A new form of nanosized $SrTiO_3$ semiconducting oxide material with an average crystal grain size of 27 nm has been synthesized using the physical high-energy ball milling technique. The unique presence of the singly charged "O^-" ions in the lattice oxygen sites of the nano-range crystal grain material has been observed in the XPS study. This unprecedented and interesting discovery has expounded on the new oxygen sensing mechanism for the near $^1/_2$ slope gradient (the best value ever reported) in the logarithmic relationship of the electrical conductance with the oxygen partial pressure. The derived $SrTiO_3$ oxygen gas sensors were found to operate at 40 °C (the lowest temperature ever reported for an $SrTiO_3$-based sensor) that is near to the human body temperature.

Introduction

The strontium titanate ($SrTiO_3$) material has been a well-researched semiconducting oxide sensing material for oxygen gas sensors. It has the advantages of being low cost and stable in both thermal and chemical atmospheres.[1] For the bulk conducting type (grain-boundary control) of this material, the sensing mechanism theory has already been well established.[1−5] In the bulk material, the carriers require energy that is high enough to overcome the Schottky barriers at the grain boundary. Hence, these sensors can only operate at a very high temperature (> 700 °C).[6,7] On the other hand; the surface conducting type material can operate at a lower temperature when the grain size is reduced to the nano range. Figure 1 illustrates the transition to grain control for the nanosized materials.[7] To the best of our knowledge, there is still no reported work on the nanosized $SrTiO_3$ oxygen-sensing materials.[2−3,8−10] We have previously reported that the physical high-energy ball milling technique is a novel and effective route to synthesize nanosized powder materials at room temperature for gas-sensing applications.[11−13] In this paper, we report on a new form of synthesized nanosized $SrTiO_3$ material that enables the derived screen-printed oxygen gas sensor to operate at 40 °C. This near-human-body temperature is much lower than that for the conventional semiconducting gas sensors (300−500 °C) and $SrTiO_3$ oxygen sensors (> 700 °C).

Experimental Section

$SrTiO_3$ nanosized powders were produced from synthesized $SrTiO_3$ and commercial $SrTiO_3$ (for comparison) at room temperature using the Fritsch Pulverizette 5-planetary-ball milling system with tungsten carbide (93 wt % WC and 6 wt % Co) vials and balls. The starting materials for the synthesized

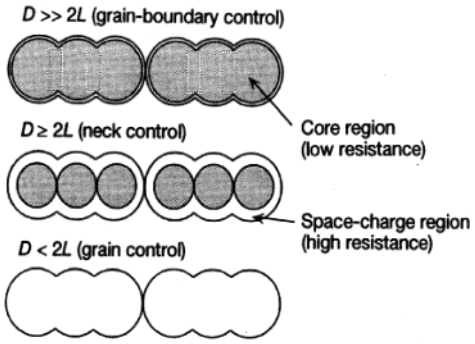

Figure 1. Schematic models for grain-size effects.[7] D: the actual grain size, L: the space-charge depth.

$SrTiO_3$ were powder of strontium oxide (SrO, 99.9% purity, density 4.700 g/cm^{-3}, Aldrich Chemical) and titanium (IV) oxide (TiO_2, 99+% purity, rutile, Johnson Matthey); and that for the commercial $SrTiO_3$ was strontium titanium oxide ($SrTiO_3$, 99+% purity, Johnson Matthey). The structures of these samples were characterized using a SHIMADZU XRD-6000 X-ray diffractometer with Cu Kαl radiation (1.54056 Å) at 40 kV and 30 mA in the range of $20° \leq 2\theta \leq 60°$ with a sweep rate of 2° per minute. Their microstructures were also studied using a JEOL JEM2010 Transmission Electron Microscope (TEM). The XPS experiments were performed using a VG ESCALAB 220-IXL instrument with an Al Kα X-ray source (1486.6 eV photons) operated at a power of 300 W. The calibration of the binding energy scale was performed with the O 1s line (531 eV).[14] The XPS spectra were analyzed using a peak synthesis program with a Shirley background and the peak fitting of the experimental data was defined by a combination of 50% Gaussian and 50% Lorentzian after the optimization. The powder samples were formed into pastes using the commercial organic binding vehicle 400 from ESL Inc., and screen-printed onto the Al_2O_3 substrates that were precoated with interdigital Au electrodes. The fabricated sensors were annealed at the temperature of 400 °C for 1 h in air. The gas

* To whom correspondence should be addressed. Tel: 065-6790-5411.Fax: 065-6791-2687. E-mail: eoktan@ntu.edu.sg (O. K. Tan).
[†] Nanyang Technological University.
[‡] Institute of Materials Research and Engineering.
[§] Xian Jiaotong University.

10.1021/jp048973z CCC: $27.50
Published on Web 06/19/2004

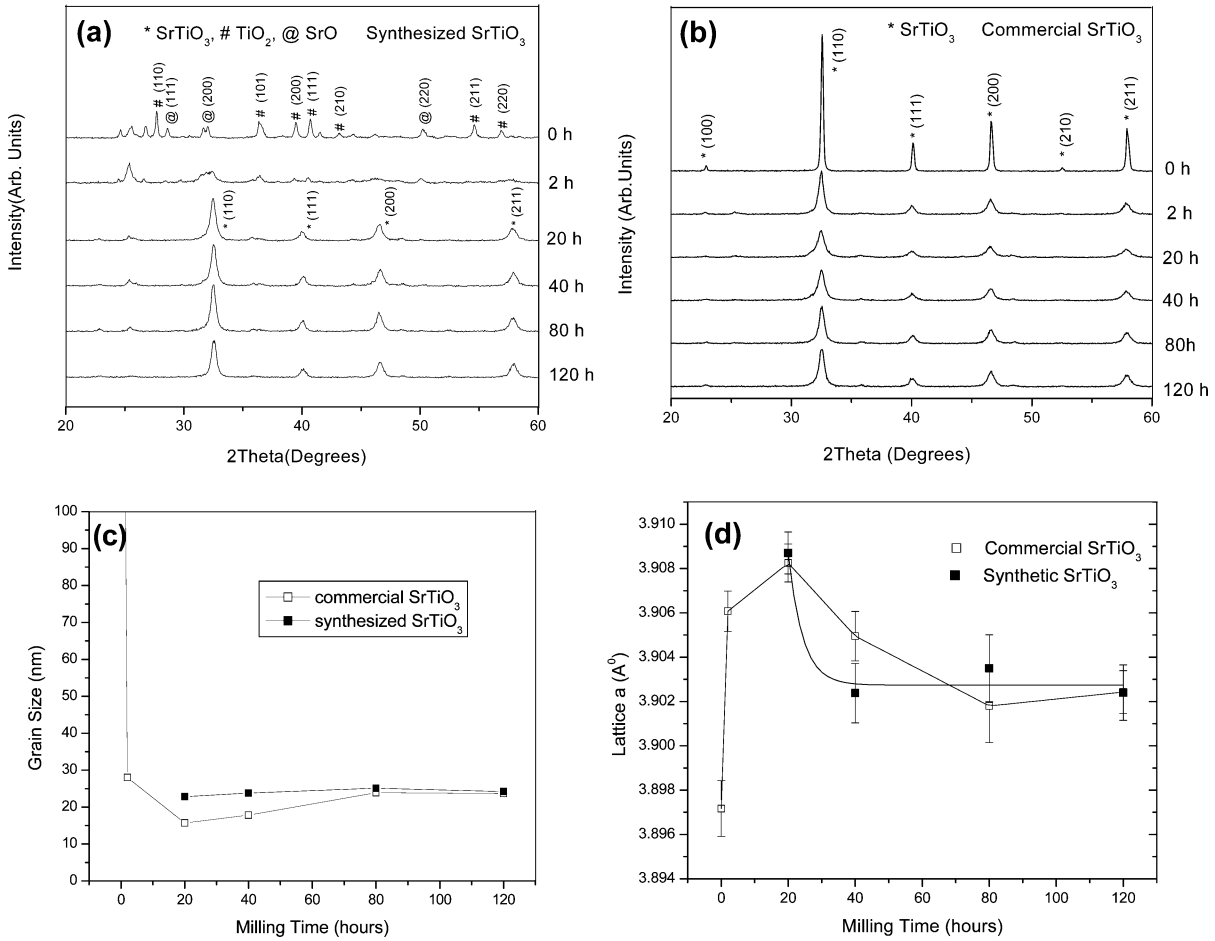

Figure 2. XRD patterns for (a) Synthesized $SrTiO_3$ and (b) Commercial $SrTiO_3$ samples for different milling times. (c) Average grain size and (d) Lattice constant ***a*** computed for different milling times.

sensing properties were characterized using a Keithley 236 source measurement unit in a custom designed gas-sensing characterization system programmed with the National Instruments' LABVIEW version 5.0. The carrier gas was nitrogen and the test gas was oxygen with different concentrations.

Results and Discussion

Material Characteristics. Figure 2(a) shows the XRD patterns for the synthesized $SrTiO_3$ samples with different milling times. For the synthesized $SrTiO_3$ material, the perovskite phase formation could be observed after 2 h of milling time. At 20 h of milling, the XRD peaks for the cubic perovskite phase of the $SrTiO_3$ structure appeared distinctively. This phase was maintained up to 120 h of milling time. The changes can be explained by the fact that during the milling process, the powders go through four different stages of the mechanical alloying process, namely (a) initial, (b) intermediate, (c) final, and (d) completion stages.[15] These involved the breaking down of the chemical bonds for the starting materials, SrO and TiO_2, followed by the forming of the new chemical bonds for the synthesized $SrTiO_3$. The completion stage for this material was observed to be at around 20 h of milling. In contrast, for the commercial $SrTiO_3$ material, the perovskite structure was maintained throughout the 120 h of milling as shown in Figure 2(b).

From the XRD peaks, the average crystal grain sizes and the lattice constants were computed for both the synthesized $SrTiO_3$ and commercial $SrTiO_3$ with different milling time and plotted in Figure 2(c) and (d), respectively. The average grain sizes were calculated using the Scherrer equation of $B = \lambda\varsigma/(d_c \cos\theta)$[15] taking into account the broadening error due to the instrument. For the synthesized $SrTiO_3$ material, these calculations were made only after the full formation of the perovskite structure at the start of 20 h of milling. The average grain size of the commercial $SrTiO_3$ decreased rapidly to a minimum at 20 h; at the same time the lattice constant increased rapidly and peaked at 20 h. It is possible that the material bonds were broken due to the large impact energy derived during high-energy ball milling, when the material is at the highest energy state. Between 20 and 120 h, the average grain sizes of the synthesized and commercial $SrTiO_3$ materials increased slightly to a stable value of 27 nm. At the same time, the lattice constants of the synthesized $SrTiO_3$ and commercial $SrTiO_3$ materials decreased gradually down to a stable value of 3.9024 Å. This is because the materials are at an extremely deformed state at 20 h of milling time, and as the surface stress of the powder particles was released, the materials changed from the unstable highest energy state at 20 h of milling time to the meta-stable state at 120 h of milling. Finally, after 120 h of ball milling, the lattice constants of the synthesized and commercial $SrTiO_3$ materials stabilized at 3.9024 Å. This value is larger than that for the commercial $SrTiO_3$ with no milling (3.8972 Å) at the stable energy state.

The TEM results for the synthesized $SrTiO_3$ material (120-h milling) are shown in Figure 3(c). The bright-field image shows a cluster of grain patterns of around 27 nm. The SAD pattern shows that the powder is a mixture of nanopolycrystalline and amorphous states. The TEM results for the commercial $SrTiO_3$

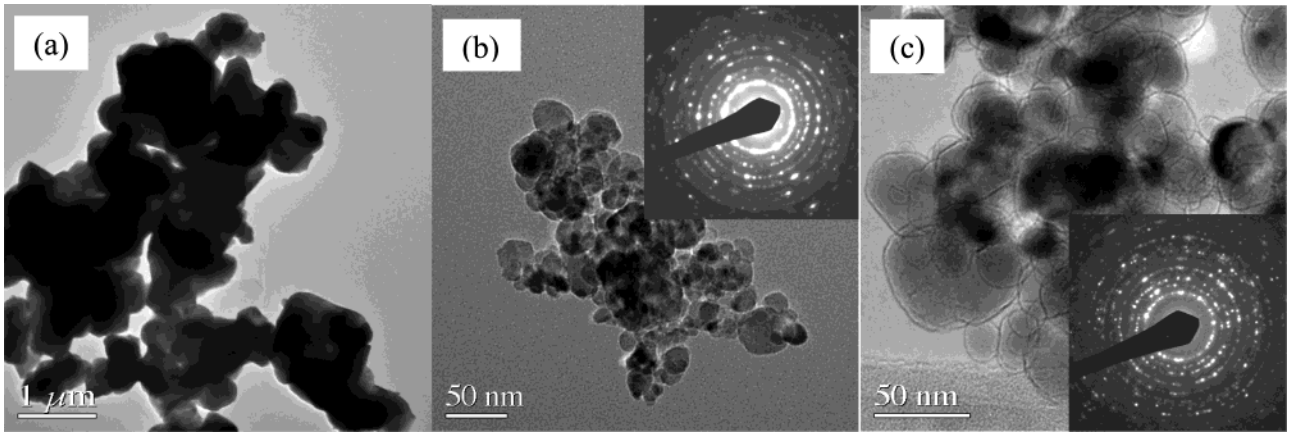

Figure 3. TEM bright-field images for (a) Commercial $SrTiO_3$ (no milling). TEM bright-field images and SAD pattern for (b) Commercial $SrTiO_3$ (120-h milling) and (c) Synthesized $SrTiO_3$ (120-h milling).

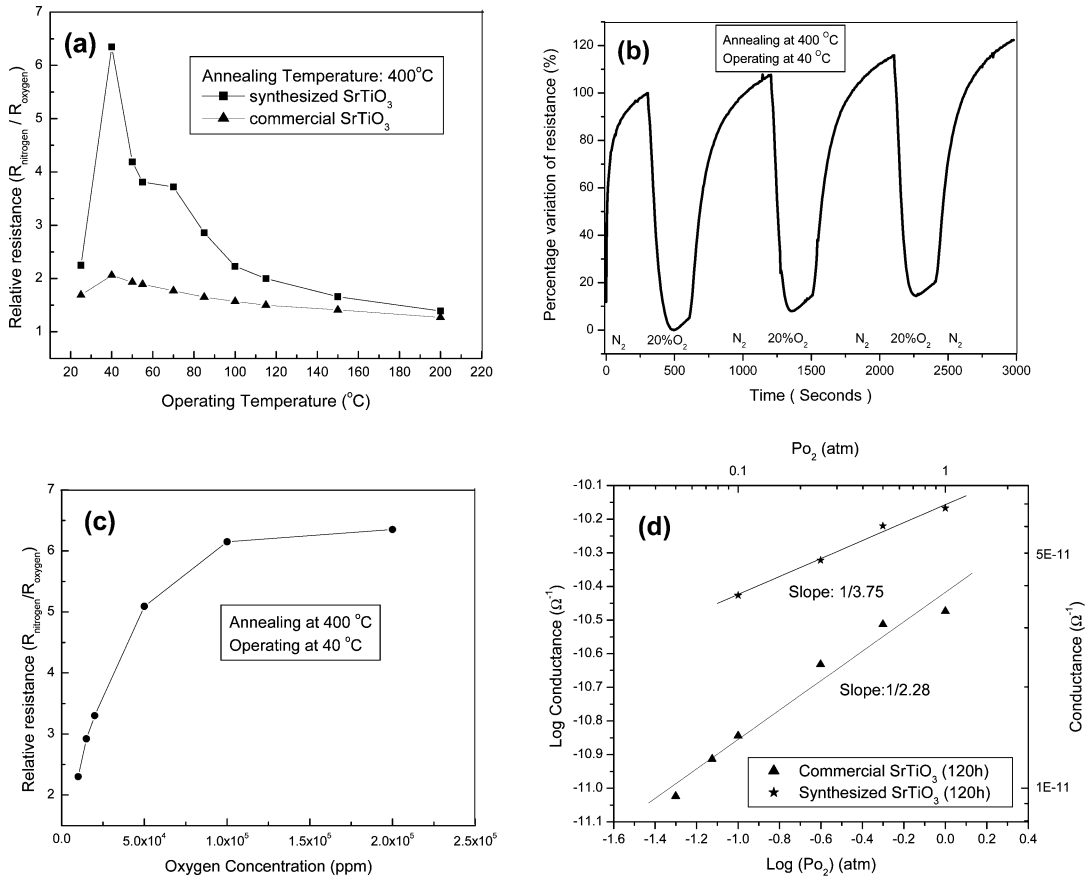

Figure 4. Sensing properties of the synthesized $SrTiO_3$-based sensor (120-h milling) annealed at 400 °C. (a) The relative resistance change to 20% O_2 in N_2 at different operating temperatures. (b) Sensing response cycles to 20% O_2 in N_2. (c) The relative resistance vs oxygen concentration. (d) P_{O_2} dependence of the electrical conductance.

material (no milling and 120-h milling) are also shown in Figure 3(a) and (b) respectively for comparison.

Sensing Properties. Figure 4 shows the sensing properties of the synthesized $SrTiO_3$-based sensor (120-h milling) annealed at 400 °C. The changes of the relative resistance ($R_{nitrogen}/R_{oxygen}$) of the devices to 20% oxygen gas in nitrogen were characterized and are depicted in Figure 4(a). Compared to the commercial $SrTiO_3$-based sensors (120-h milling), the relative resistance change for the synthesized $SrTiO_3$-based sensor (120-h milling) was observed to be more than 3 times better. It is noted that the commercial $SrTiO_3$-based sensor (no milling) exhibited no sensing property as it is still an insulating material. The optimal relative resistance value of 6.35 is obtained for the synthesized $SrTiO_3$-based sensor (120-h milling) operating at 40 °C. This value is comparable to the reported relative resistance of doped $SrTiO_3$ series oxygen gas sensors with operating temperature at 700−800 °C.[8−9,16] We believed that this 40-°C optimum operating temperature is the lowest temperature ever reported for the $SrTiO_3$ oxygen gas sensors.[6] The synthesized $SrTiO_3$-based sensor (120-h milling) operating at 40 °C to 20% O_2 in N_2 also exhibited a good repeatable response property as shown in Figure 4(b). The detection ranges of oxygen concentration characterized for the synthesized $SrTiO_3$-based sensor (120-h milling) operating at 40 °C is from 10^4 to 2×10^5 ppm in N_2 (or 1−20% O_2) as shown in Figure 4(c). This provides a wide concentration range for these oxygen sensor devices operating

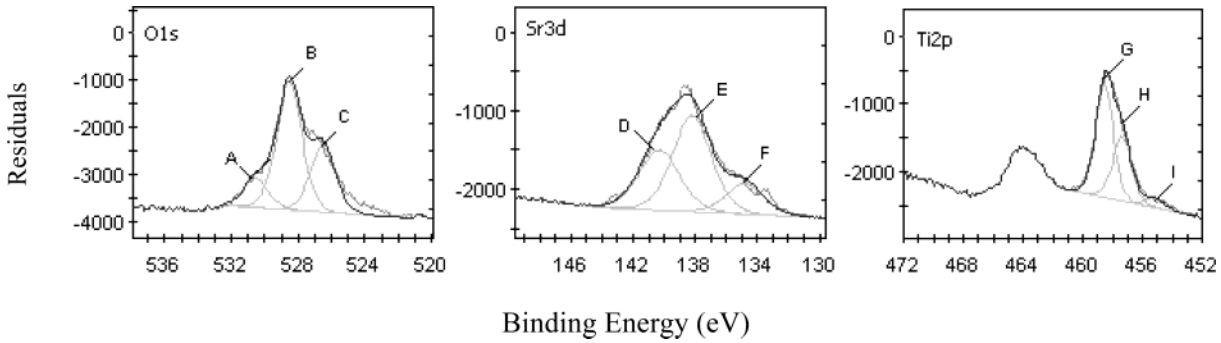

Figure 5. The O 1s, Sr 3d, and Ti 2p XPS spectra at 25 °C for the synthesized $SrTiO_3$ (120-h milling).

TABLE 1: Average Core Level Binding Energies (BEs)[17] and Average Atomic Concentrations (At%) of O 1s, Sr 3d, Ti $2p_{3/2}$, and C 1s for Synthesized $SrTiO_3$ (120-h milling)[a]

	O 1s			Sr 3d			Ti $2p_{3/2}$			
	O^-_{ads}	O^{2-}_{latt}	O^-_{latt}	Sr $3d_{3/2}$	Sr $3d_{5/2}$		Ti^{4+}	Ti^{3+}	Ti^{2+}	C 1s
main peak (eV)	A: 530.5	B: 528.5	C: ***526.5***	D: 140.3	E: 138.2	F: 134.8	G: 458.5	H: 457.3	I: 455.0	J: 284.3
At (%)	4.6	20.5	***10.7***	12.3	18.5	5.5	13.1	***8.6***	***1.3***	4.9
					24.0			***23.0***		

[a] (O^-_{ads}: the adsorbed "O^-" ions on surface; O^{2-}_{latt}: the lattice "O^{2-}" ions; O^-_{latt}: the lattice "O^-" ions)

at near-human-body temperature. Figure 4 (d) shows the oxygen partial pressure Po_2-dependence of the synthetic $SrTiO_3$-based (120-h milling) sensor and the commercial $SrTiO_3$-based (120-h milling) sensor operating at 40 °C. The slope gradients in the logarithmic relationship of the electrical conductance with the oxygen partial pressure are 1/2.28 and 1/3.75, respectively.

Sensing Mechanism and XPS Analysis. In general, the semiconducting oxide material is a nonstoichiometric oxide, for example, an oxygen deficient oxide containing oxygen vacancies. These oxygen vacancies diffuse readily between the interior and the surface of the grains when exposed in a high ambient temperature (700−1100 °C). The basic reaction between the regular oxygen site (Oo^x), oxygen molecules in the gas phase ($O_2^{(g)}$), and the oxygen vacancy ($Vo^{\bullet\bullet}$) in the bulk can be expressed as:[6]

$$Oo^x \leftrightarrow Vo^{\bullet\bullet} + 2e' + 1/2O_2^{(g)} \quad (1)$$

The well-known relationship between the electrical conductance, σ, of a sensor device and the oxygen partial pressure, P_{O_2}, can be written as:

$$\sigma = A\exp(-E_A/KT)P_{O_2}^{1/m} \quad (2)$$

where E_A is the activation energy that represents the sensitivity of σ to temperature changes. The absolute value of $1/m$ represents the sensitivity of σ to change in the oxygen partial pressure. It depends on the dominating defects involved in the reaction between the oxygen gas molecules and the sensor. The sign of $1/m$ depends on the type of conduction. For p-type conduction, the value of $1/m$ is positive, and for n-type conduction it is negative. It is believed that sensing materials with a small E_A value and a large $1/m$ value are most suitable to achieve good sensitivity with respect to the changes in the oxygen pressure. In Figure 4 (d), the slope gradients of the log σ to log Po_2 are positive for the synthetic $SrTiO_3$-based (120-h milling) sensor and the commercial $SrTiO_3$-based (120-h milling) sensor. Hence they are both p-type.

The detection range of 0.03 to 1 atm P_{O_2} for the synthesized $SrTiO_3$-based (120-h milling) oxygen gas sensors can be classified as the high P_{O_2} region ($P_{O_2} > 10^{-4}$ atm). In this high P_{O_2} region there are possibly two types of sensing mechanisms present in the oxygen sensors:

$$\text{Type I:}\quad 1/2O_2^{(g)} + Vo^{\bullet\bullet} \leftrightarrow Oo^x + 2h^{\bullet} \quad (3)$$

$$p = K_1[Vo^{\bullet\bullet}]^{1/2}P_{O_2}^{1/4} \quad (4)$$

$$\log\sigma \propto {}^1/_4 \log P_{O_2} \quad (5)$$

$$\text{Type II:}\quad 1/2O_2^{(g)} + V_O^{\bullet} \leftrightarrow Oo^x + h^{\bullet} \quad (6)$$

$$p = K_2[V_O^{\bullet}]P_{O_2}^{1/2} \quad (7)$$

$$\log\sigma \propto {}^1/_2 \log P_{O_2} \quad (8)$$

where K_1 and K_2 are the equilibrium constant for the respective reaction, and $p \equiv [h^{\bullet}]$ represents the concentration of the holes in the material.

The slope gradient of 1/3.75 for the commercial $SrTiO_3$-based (120-h milling) sensor shown in Figure 4 (d) is very near $^1/_4$, and hence it mainly exhibits the Type I mechanism. Interestingly, the slope gradient of 1/2.28 for the synthesized $SrTiO_3$-based (120-h milling) sensor shown in Figure 4 (d) is very near $^1/_2$, hence it predominantly has the Type II mechanism. We believe this slope gradient that is near to $^1/_2$ is the best value ever achieved; all other reported values are in the $^1/_4$ value range and hence exhibit a Type I sensing mechanism.[6] These sensing mechanisms have been further confirmed in the XPS experiments.

We postulate that the synthesized $SrTiO_3$ material structure can take on three possible forms:

$$\text{Form I: } \overset{+2}{Sr}\,\overset{+4}{Ti}\,\overset{[(-2*3)]}{O_3} \qquad [Sr^{2+}] + [Ti^{4+}] = 3[O^{2-}] \quad (9)$$

$$\text{Form II: } \overset{+2}{Sr}\,\overset{+3}{Ti}\,\overset{[(-2*2)+(-1*1)]}{O_3} \qquad [Sr^{2+}] + [Ti^{3+}] = 2[O^{2-}] + [O^-] \quad (10)$$

$$[Ti3^+]/[O^-]_{lattII} = 1/1 \quad (11)$$

$$\text{Form III: } \overset{+2}{Sr}\,\overset{+2}{Ti}\,\overset{[(-2*1)+(-1*2)]}{O_3} \qquad [Sr^{2+}] + [Ti^{2+}] = [O^{2-}] + 2[O^-] \quad (12)$$

$$[Ti2^+]/[O^-]_{lattIII} = 1/2 \quad (13)$$

where the singly charged lattice oxygen ion "O^-" is also present in Forms II or III besides the well-known doubly charged lattice oxygen ion "O^{2-}". The $[O^-]_{lattII}$ and $[O^-]_{lattIII}$ denote the concentration of the "O^-" ions of the lattice oxygen in Form II and Form III of $SrTiO_3$ respectively.

All Ti^{2+}, Ti^{3+}, Ti^{4+}, O^{2-}, and O^- structures were found to exist in the synthesized $SrTiO_3$ XRD peak list at a 2-h milling time. The O^- can occur in the form of SrO_2 in the synthesized $SrTiO_3$. The XPS experiments confirm the presence of Ti^{2+}, Ti^{3+}, Ti^{4+}, O^{2-}, and O^- ions in the synthesized $SrTiO_3$ material (120-h milling) and elucidate the sensing mechanism of the synthesized $SrTiO_3$-based oxygen gas sensor. Figure 5 shows the XPS spectra for the O 1s, Sr 3d, and Ti 2p regions of synthesized $SrTiO_3$ (120-h milling) at 25 °C, and the detailed XPS information is collated in Table 1.

The synthesized $SrTiO_3$ (120-h milling) material was discovered to possess a unique Peak C in O 1s representing the "O^-" ions of the lattice oxygen. Its binding energy position at 526.5 eV has been confirmed and is consistent with that for the "O^-" ions of the lattice oxygen in the commercial strontium peroxide (SrO_2, density 4.560 g/cm^{-3}, Aldrich Chemical) obtained at 525.7 eV.

If Form II and Form III exist in the synthesized $SrTiO_3$, then

$$[O^-]_{latt} = [O^-]_{lattII} + [O^-]_{lattIII} = [Ti^{3+}] + 2\,[Ti^{2+}] \quad (14)$$

From Table 1, $[O^-]_{latt}$ has a value of 10.7 At% and the combined ($[Ti^{3+}] + 2\,[Ti^{2+}]$) value is 11.2 At%. This verifies that the two values are quite consistent and that eq 14 is true. Similarly, the mole ratio of Sr to Ti of the synthesized $SrTiO_3$ (120-h milling) is near 1. The average atomic concentrations of Sr and Ti are calculated at 24.0 At% and 23.0 At%, from Sr $3d_{5/2}$ and Ti $2p_{3/2}$, respectively.[14] The XPS results show that the synthesized $SrTiO_3$ (120-h milling) has predominantly Form II and Form III. The existence of these two forms provides good sensitivity for the derived sensors for oxygen sensing at near-human-body temperature.

Conclusions

The new form of nanosized $SrTiO_3$ material has been synthesized using the high-energy ball milling technique. The average crystal grain size is 27 nm and the $SrTiO_3$ lattice structure of the synthesized $SrTiO_3$ has been found to be 3.9024 Å. The thick-film screen printed synthesized $SrTiO_3$-based sensors were found to have the relative resistance ($R_{nitrogen}/R_{oxygen}$) value of 6.35 to 20% of oxygen in nitrogen at the operating temperature of 40 °C. This operating temperature is much lower than that of the conventional semiconducting oxygen gas sensors (300−500 °C)[6] and $SrTiO_3$ oxygen sensors (> 700 °C). The XPS results reviewed the existence of the singly charged "O^-" ions in the lattice oxygen sites of the new synthesized nanosized $SrTiO_3$ material and explain the new oxygen sensing mechanism of the near $^1/_2$ slope gradient (the best value ever reported[6]) for the logarithmic relationship of the electrical conductance to the oxygen partial pressure.

References and Notes

(1) Menesklou, W.; Hans-Jürgen Schreiner; Härdtl, K. H.; Ivers-Tiffée, E. *Sens. Actuators B* **1999**, *59*, 184−189.
(2) Moos, R.; Menesklou, W.; Hans-Jürgen, S.; Härdtl, K. H. *Sens. Actuators B* **2000**, *67*, 178−183.
(3) Feighery, A. J.; Abrantes, J. C. C.; Labrincha, J. A.; Ferreira, J. M. F.; Frade, J. R. *Sens. Actuators B* **2001**, *75*, 88−94.
(4) Ohly, C.; Hoffmann-Eifert, S.; Szot, K.; Waser, R. *J. Eur. Ceram. Soc*. **2001**, *21*, 1673−1676.
(5) Costa, M. E. V.; Jurado, J. R.; Colomer, M. T.; Frade, J. R. *J. Eur. Ceram. Soc.* **1999**, *19*, 769−772.
(6) Xu, Y. L.; Zhou, X. H.; Sørensen, O. T. *Sens. Actuators B* **2000**, *65*, 2−4.
(7) Shimizu, Y.; Egashira, M. *MRS Bull.* **1999**, June, 18−24.
(8) Zhou, X. H.; Sørensen, O. T.; Xu, Y. L. *Sens. Actuators B* **1997**, *41*, 177−182.
(9) Zhou, X. H.; Sørensen, O. T.; Cao, Q. X.; Xu, Y. L. *Sens. Actuators B* **2000**, *65*, 52−54.
(10) Ding, T. Z.; Jia, W. G. *Sens. Actuators B* **2002**, *82*, 52−54.
(11) Cao, W.; Tan, O. K.; Zhu, W.; Pan, J.; Jiang, B. *IEEE Sensors Journal* **2003**, *3*, 421−434.
(12) Tan, O. K.; Cao, W.; Zhu, W. *Sens. Actuators B* **2000**, *63*, 129−134.
(13) Cao, W.; Tan, O. K.; Zhu, W.; Jiang, B. *J. Solid State Chem.* **2000**, *155*, 320−325.
(14) van der Heide, P. A. W.; Jiang, Q. D.; Kim, Y. S.; Rabalais, J. W. *Surf. Sci*. **2001**, *473*, 59−70.
(15) Lü, L.; Lai, M. O. *Mechanical Alloying*; Kluwer Academic Publishers: 1998.
(16) Zheng, H.; Sørensen, O. T. *Sens. Actuators B* **2000**, *65*, 299−301.
(17) Moulder, J. F.; Stickle, W. F.; Sobol, P. E.; Bomben, K. *Physical Electronics*, 2nd ed.; J. Chastain: Perkin-Elmer Corporation, 1992.